Journal of Alloys and Compounds 480 (2009) 485–493

Contents lists available at ScienceDirect

Journal of Alloys and Compounds

journal homepage: www.elsevier.com/locate/jallcom

Microstructural evolution during upward and downward transient directional solidification of hypomonotectic and monotectic Al–Bi alloys

Adrina P. Silva, José E. Spinelli, Amauri Garcia*

Department of Materials Engineering, University of Campinas – UNICAMP, PO Box 6122, 13083-970 Campinas, SP, Brazil

ARTICLE INFO

Article history:
Received 4 November 2008
Received in revised form 19 January 2009
Accepted 22 January 2009
Available online 6 February 2009

Keywords:
Metals and alloys
Microstructure
Thermal analysis

ABSTRACT

Upward directional unsteady-state solidification experiments were performed with both a hypomonotectic Al–2.0 wt% Bi alloy and a monotectic Al–3.2 wt% Bi alloy. Besides, the monotectic composition (3.2 wt% Bi) was directionally solidified under downward transient heat flow conditions, which enables the effects of melt convection on the final microstructure to be evaluated since the collective downward movement of Bi-rich particles is favored in such case. This is due to the density differences between the two coexisting liquid phases. The thermal parameters such as cooling rate, growth rate and thermal gradient were experimentally determined by data collected from cooling curves recorded along the casting length. The monotectic features observed in the Al–3.2 wt% Bi alloy castings, i.e. the interphase spacing and Bi-rich particles diameter were correlated with the growth rate and thermal gradient. The cell spacing was experimentally determined for the Al–2.0 wt% Bi alloy as a function of both the cooling rate and tip growth rate. These experimental data were compared with the main predictive cellular growth models from the literature. A comparison between upward and downward unsteady-state solidification results for the interphase spacing and Bi-rich particles diameter has also been conducted.

1. Introduction

Aluminum alloys dispersed with bismuth show promising tribological applications in automotive components. Such dispersions of low melting temperature elements decrease hardness and flow easily under sliding conditions, resulting in favorable tribological behavior [1]. Recent investigations pointed out the possibility of fabrication of porous aluminum with deep pores by using monotectic alloys and electrochemical etching. Porous materials present many advantages which include large surface area with respect to their volume, permeation of fluids, ability to hold fluid in their pores and high strength to weight ratio [2,3]. By using monotectic materials for fabrication of pores, it is possible to produce anisotropic porous media with pores sizes of 5–20 μm. This size is smaller than that obtained through classic procedures of porous materials fabrication.

When a monotectic Al–Bi alloy is cooled from the single phase L_1 to the monotectic temperature (T_M), the liquid decomposes in equilibrium simultaneously into a solid phase (S_1) of nearly pure Al and a liquid L_2. There is typically a wide temperature interval between the monotectic horizontal line and the terminal eutectic reaction [4]. As a consequence, the product of the monotectic reaction remains in $S_1 + L_2$ field for relatively long times during subsequent cooling, being susceptible to perturbation, spheroidization and ripening.

According to Zhao et al. [5] a liquid-to-liquid decomposition in monotectic alloys begins with the nucleation of the liquid minority phase in the form of droplets. These droplets grow by diffusion of solute in the matrix. They can also settle due to gravity or migrate due to a temperature or a concentration gradient. It is also expected a macrosegregation profile to be formed during solidification of monotectic castings since large composition and density differences exits between the two liquid phases. Ludwig et al. [6] simulated the occurrence of convection phenomena during directional solidification of an Al–10 wt% Bi alloy. They examined both the droplet motion and its influence on the final phase distribution.

Much research has been devoted in order to better comprehend the distinct morphologies obtained by monotectic reaction [4–12]. As found in other researches, Ratke and Müller [7,8] assume that the phase spacing evolution in the monotectic Al–Bi alloy follows the classical relationship used for eutectics: $\lambda^2 v = C$, where v is the solidification velocity and C a constant value. It is also highlighted that published values of C for Al–Bi monotectic differ up to one order of magnitude (between 10^{-14} and 10^{-15}). In a recent study, Silva et al. [13] have found a C-value of 1.7×10^{-12} concerning non-steady solidification conditions, which is about two orders of magnitude higher than those reported for the steady-state regime at any given growth rate. However, Carlberg and Bergman [9] reported that the

* Corresponding author. Tel.: +55 19 3521 3320; fax: +55 19 3289 3722.
E-mail address: amaurig@fem.unicamp.br (A. Garcia).

0925-8388/$ – see front matter © 2009 Elsevier B.V. All rights reserved.
doi:10.1016/j.jallcom.2009.01.105

relationship between fiber spacing λ and solidification thermal variables (G and v) for monotectics could be not only similar to the growth law for some irregular eutectics but also very similar to expressions for dendritic growth.

Ratke [14] proposed a new theoretical approach considering an additional mode of mass transport ahead of the monotectic solidification front, i.e. the Marangoni convection. Such description provides a clear difference between monotectic and eutectic solidification. The former encompasses a liquid phase state of the L_2 phase growing simultaneously with a perfectly pure solid matrix. Convection is caused by thermocapilarity effects at the interface with the liquid phase. The theoretical results show a new relationship between interphase spacing and solidification velocity as well as a clear dependence of this kind of relationship on the temperature gradient ahead of the solidification front. Further, larger interphase spacing was predicted as a result of the flow induced by this surface tension driven convection.

Yang and Liu [11] have reported that both the spacing and diameter of Bi fibers decreased as a consequence of a transverse magnetic field imposed during solidification of a monotectic Al–6.5 wt% Bi alloy. The difficulty of producing homogeneous microstructures in monotectic alloys is stated as a problem that has delayed the utilization of monotectics as industrial materials. Thermal and solutal gradients induced in the melt during solidification are considered the main effects to cause microstructure coarsening.

In order to investigate the influence of gravity on the microstructure of the Cu–Pb monotectic alloy, Aoi et al. [15] carried out upward and downward unidirectional solidification experiments. They found that the resultant microstructure is not dependent on the growth direction, which means that, according to these authors, gravity does not significantly affect the solute redistribution during the monotectic growth.

Reuβ et al. [16] examined the microstructure evolution of a rapidly directionally solidified hypermonotectic Al–5 wt% Bi alloy. Variable cooling rates were imposed in a range from 2 to 20 K/s by using mold materials with very different thermal conductivities, such as ceramics, graphite, titanium, steel and copper. It was found that the average diameter of the particles increases with decreasing cooling rates. A power function is proposed in order to correlate the diameter of the particles and the cooling rate, given by $d = c(\mathrm{d}T/\mathrm{d}t)^n$, where d is the particle diameter, $\mathrm{d}T/\mathrm{d}t$ is the cooling rate, $n = -0.43$ (slope of the fit to the experimental values) and c is a constant.

Although several works cover the analysis of monotectic or off-monotectic compositions in the Al–Bi system [4,6–8,10,11,13,16], little attention has been given to the microstructure evolution of hypomonotectic alloys. Most of the aforementioned studies have used Bridgman-type resistance heated furnaces to produce the directionally solidified monotectic samples. In contrast, there is a lack of consistent studies and experimental reports on the microstructural development of monotectic and off-monotectic Al–Bi alloys during transient heat flow conditions, which are of prime importance since this class of heat flow encompasses the majority of solidification industrial processes.

In the present study, upward directional unsteady-state solidification experiments were performed with both a hypomonotectic Al–2.0 wt% Bi alloy and a monotectic Al–3.2 wt% Bi alloy. The monotectic composition (3.2 wt% Bi) was also directionally solidified under downward transient heat flow conditions, in order to permit the effect of melt convection on the final microstructure to be evaluated. This study focuses on the influence of solidification thermal parameters (thermal gradient and growth rate) on the microstructural evolution of both the hypomonotectic and the monotectic alloys and on the effect of growth direction with respect to the gravity vector on the interphase spacing and on the Bi-rich droplets diameter of the monotectic Al–Bi composition.

2. Theoretical models for cellular growth

Hunt [17] and Kurz and Fisher [18,19] have proposed detailed theoretical models to characterize cells and primary dendrite spacings during steady-state growth conditions, which are based only on diffusive transport. Hunt has based his model on two major assumptions: a dendrite or cell profile approximated by a smooth steady-state shape even when dendrite arms have been formed and constant temperature and liquid composition in the direction normal to the primary dendritic growth direction. Kurz and Fisher have assumed that the overall morphology of the dendrite (tip and trunk) can be approximated by an ellipsoid. They consider that this shape has the advantage over the paraboloid that a parabolic-like form exists at the tip, while the lower part of the ellipsoid better represents the real dendrite. The equations representing these two theories can be expressed, respectively by

$$\lambda_1 = 2.83[\Gamma m_L C_0(1-k_0)D]^{1/4} G_L^{-1/2} V_L^{-1/4} \quad \text{(Hunt, cellular/dendritic)} \qquad (1)$$

$$\lambda_1 = 4.3\left(\frac{\Gamma \Delta T D}{k_0}\right)^{1/4} G_L^{-1/2} V_L^{-1/4} \quad \text{(Kurz and Fisher, cellular/dendritic)} \qquad (2)$$

Trivedi [20] proposed a theoretical model based on the theoretical assumptions proposed by Hunt [17]. A constant L_T was included in the equation and it is dependent on the harmonic perturbations of the system. The author assumed L_T equal to 28. The following equation represents the Trivedi's model:

$$\lambda_1 = 2.83[L_T \Gamma m_L C_0(1-k_0)D]^{1/4} G_L^{-1/2} V_L^{-1/4} \quad \text{(Trivedi, cellular/dendritic)} \qquad (3)$$

Hunt and Lu [21] have proposed a numerical model of cellular and dendritic growth, based also on purely diffusive growth, which is able to predict cellular and dendritic spacings, undercooling and the transition between structures. The model solves the solute transport problem in the liquid using a time-dependent finite difference method. Heat flow is included by assuming a moving linear temperature field, with the difference in thermal conductivity between the two phases being neglected, as is latent heat evolution. Surface energy and surface energy anisotropy of the solid/liquid interface are incorporated. Solution to the diffusion problem and the prediction of the self-consistent shape are made using a fully implicit control volume method. The model describes steady-state and non-steady-state growth of an axisymmetric cell or dendrite, and is given for cellular growth by the following relationship:

$$\lambda_1 = 8.18 k_0^{-0.745}\left(\frac{\Gamma}{\Delta T}\right)^{0.41} D^{0.59} V_L^{-0.59} \qquad (4)$$

where λ_1 is the cellular spacing, Γ is the Gibbs–Thomson coefficient, m_L is the liquidus line slope, C_0 is the alloy composition, k_0 is the solute partition coefficient, D is the liquid solute diffusivity, ΔT is the difference between the liquidus and monotectic equilibrium temperatures, V_L is the cell tip growth rate and G_L is the temperature gradient ahead the cell tip. They evaluated the lower and upper limits of the spacings within which an array can be stable, and proposed that the upper limit should be twice the lower one.

The theoretical predictions furnished by the aforementioned models will be compared with experimental results obtained in the present study for the hypomonotectic Al–2.0 wt% Bi alloy. The

Table 1
Thermophysical properties of the Al–2 wt% Bi hypomonotectic alloy.

Properties	Symbol	Al–2.0 wt% Bi
Solute diffusivity ($m^2\,s^{-1}$)	D	3.9×10^{-9}
Gibbs–Thomson coefficient (mK)	Γ	9.8×10^{-7}
Liquidus temperature (°C)	T_L	659
Monotectic temperature (°C)	T_M	658
Liquidus slope (°C wt pct^{-1})	m_L	0.73
Partition coefficient	k_0	0.141

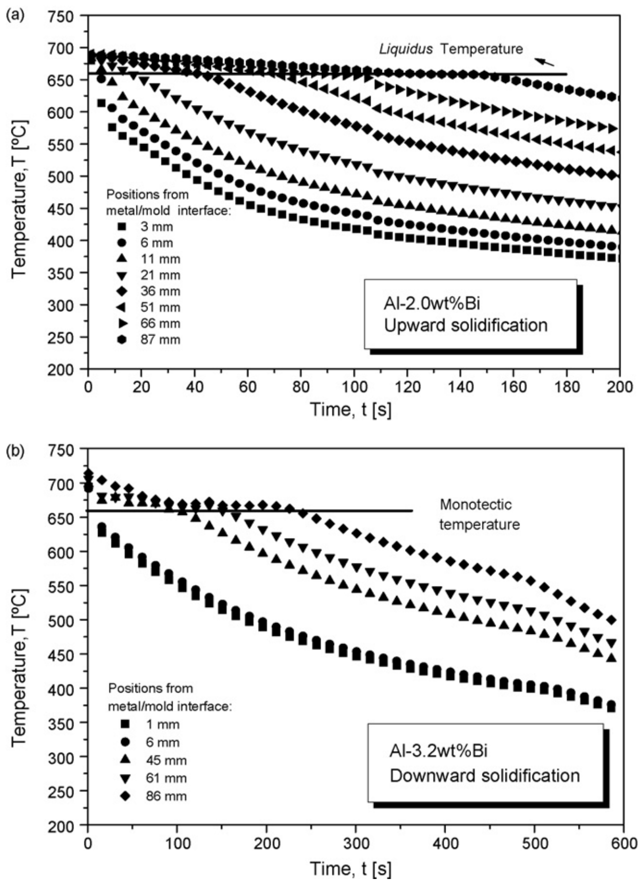

Fig. 1. Experimental cooling curves obtained for (a) Al–2.0 wt% Bi alloy solidified upwards and (b) Al–3.2 wt% Bi alloy solidified downwards.

liquidus temperature, the liquidus line slope, the monotectic temperature and the partition coefficient have been obtained in the present study by ThermoCalc[1] computations, while the solute diffusivity and the Gibbs–Thomson coefficient are those reported by Derby and Favier [10]. The necessary thermophysical properties of this alloy are summarized in Table 1.

3. Experimental procedure

The experimental setups used in the upward and downward transient directional solidification experiments have been detailed in previous articles [13,22]. Heat is directionally extracted only through the water-cooled system, which permits a wide range of solidification thermal parameters to be analyzed. The experiments which were performed with the Al–3.2 wt% Bi monotectic alloy had the initial melt temperature (T_p) adjusted at about 5% above the monotectic temperature (T_M) while the experiment performed with the Al–2.0 wt% Bi was started with 5% above the *liquidus* temperature (T_L). The enlarged partial phase diagram of the Al–Bi system, has been shown in a previous study [13] and permits a clear visualization of phases and transformation temperatures in the hypomonotectic range of Al–Bi alloys.

[1] ThermoCalc software is an exclusive copyright property of the STT Foundation (Foundation of Computational Thermodynamics, Stockholm, Sweden).

Continuous temperature measurements in the casting were monitored during solidification via the output of fine type K thermocouples (made from 0.2 mm diameter wire), which were positioned at 5–8 different positions along the casting length from the cooled surface. The thermocouples were calibrated at the melting point of aluminum exhibiting fluctuations of about 1 °C. All of the thermocouples were connected by coaxial cables to a data logger interfaced with a computer, and the temperature data, read at intervals of 0.5 s, were automatically acquired.

The cylindrical ingots were subsequently sectioned along its vertical axis, ground and etched with an acid solution to reveal the macrostructure (Poulton's reagent: 5 mL H_2O; 5 mL HF–48%; 30 mL HNO_3; 60 mL HCl). In order to perform a metallographic examination of the alloys with monotectic composition, selected longitudinal sections (parallel to the growth direction) along the casting length were electropolished and etched (a solution of 0.5% HF in water). The same procedure was adopted for the Al–2.0 wt% Bi alloy sample which was solidified vertically upwards despite examining selected cross-sections. Image processing systems were used to measure the interphase spacing (λ). It was measured along the casting longitudinal section by averaging the horizontal distance between the Bi particles, adopting as reference the center of each particle. The evolution of Bi-rich particles size (droplet diameter: d) along the casting length was also determined. The method used for measuring the cell spacing (λ_1) on transverse sections of the Al–2.0 wt% Bi casting was the triangle method [23]. About 50 independent readings for each selected position were obtained for all aforementioned cases.

4. Results and discussion

The acquired cooling curves are shown in Fig. 1. These curves correspond to the thermal responses of the thermocouples inserted along the length of two directionally solidified castings, i.e. the Al–3.2 wt% Bi alloy (downwards) and the Al–2.0 wt% Bi alloy (upwards).

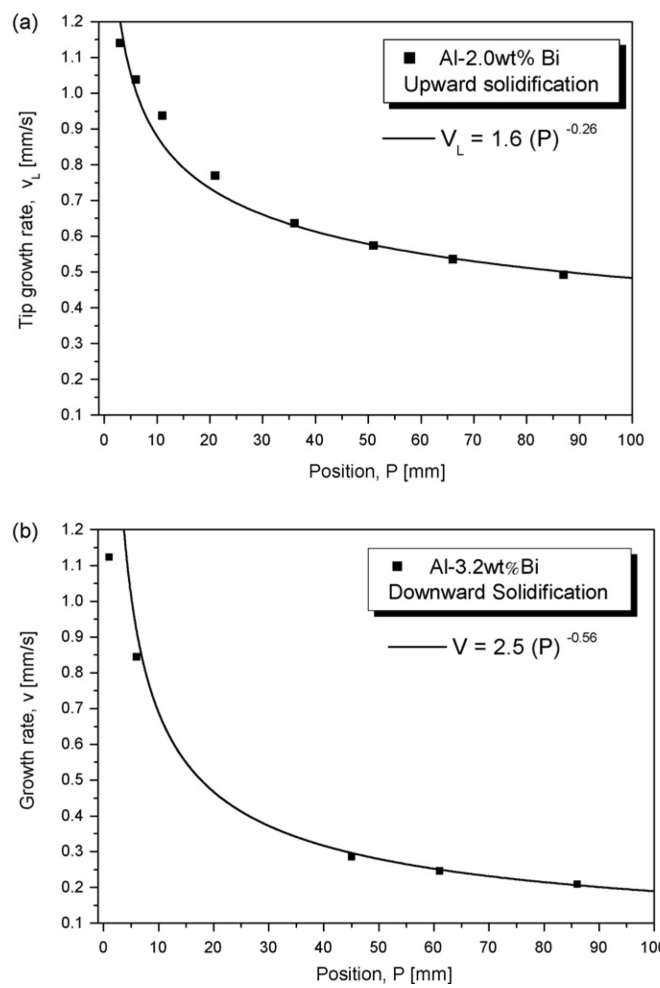

Fig. 2. Experimental growth rate as a function of position from the cooled surface for (a) Al–2.0 wt% Bi alloy solidified upwards and (b) Al–3.2 wt% Bi alloy solidified downwards.

The thermocouples readings of each experiment have been used to generate a plot of position from the metal/mold interface as a function of time corresponding to either the monotectic front (Al–3.2 wt% Bi) or the *liquidus* isotherm (Al–2.0 wt% Bi) passing by each thermocouple. A curve fitting technique on these experimental points has generated a power function of position as a function of time. The derivatives of these functions with respect to time have yielded values for both the monotectic front growth rate (v) and the tip growth rate (v_L), as shown in Fig. 2.

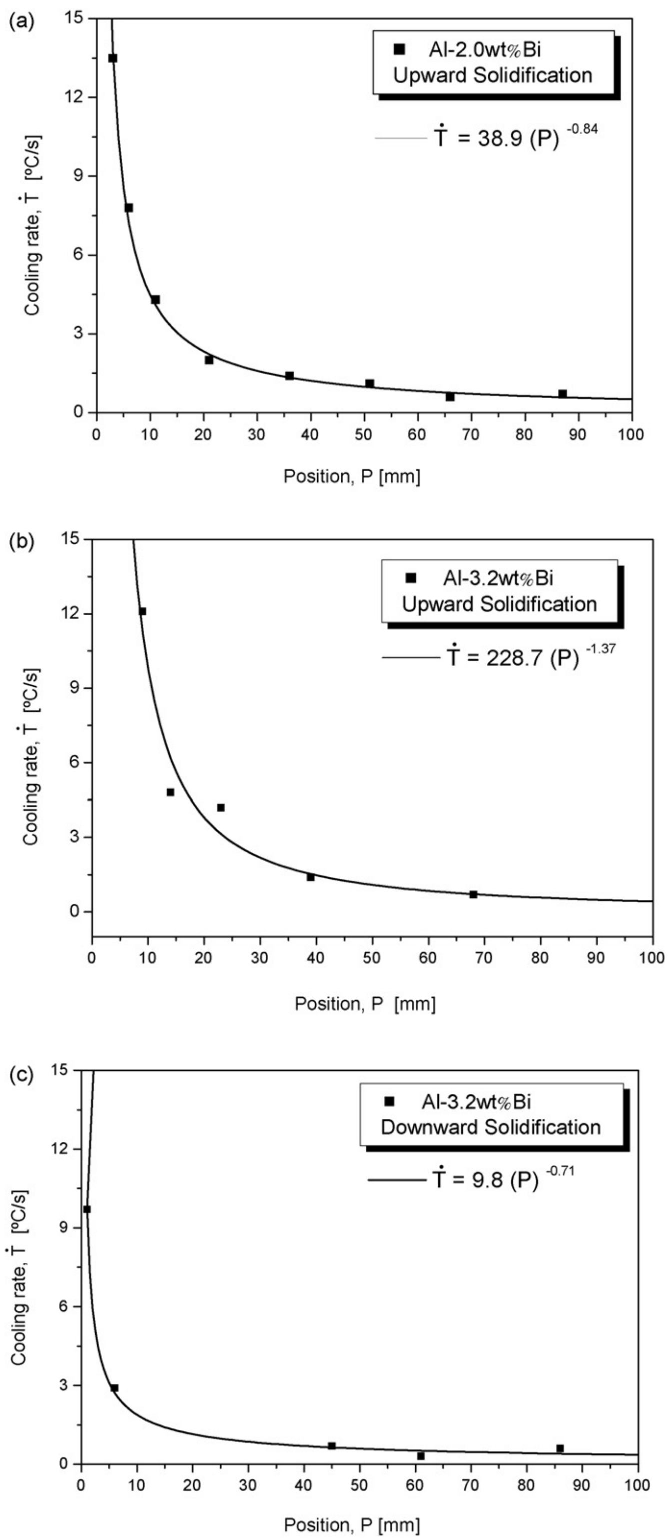

Fig. 3. Experimental cooling rate as a function of position from the cooled surface for (a) Al–2.0 wt% Bi, (b) Al–3.2 wt% Bi alloys solidified upwards and (c) Al–3.2 wt% Bi alloy solidified downwards.

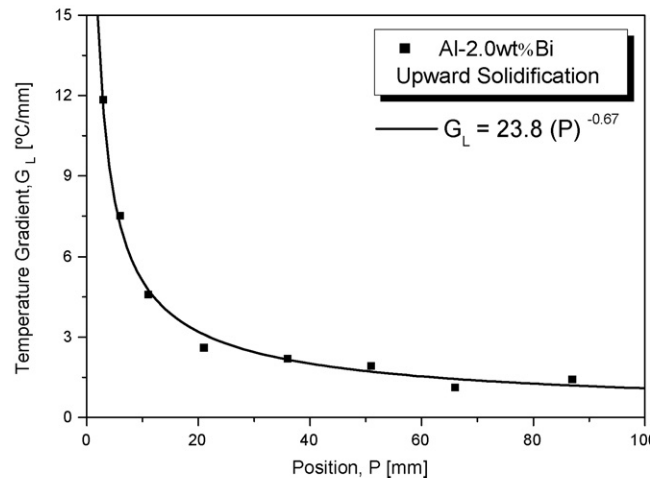

Fig. 4. Temperature gradient as a function of position from the cooled surface for the Al–2.0 wt% Bi alloy solidified upwards.

The cooling rate was determined by computing the slope of the experimental cooling curve considering the thermal data recorded immediately after the passing of the respective fronts by each thermocouple, i.e. the *liquidus* front in the case of Al–2.0 wt% Bi alloy and the monotectic front for Al–3.2 wt% Bi alloy. These curves can be seen in Fig. 3.

Solidification contraction associated with the casting weight in conditions of downward growth contributes to the detachment of the ingot surface from the cooled mold in the early beginning of solidification. As a consequence, lower growth rates (Fig. 2) and cooling rates (Fig. 3) can be seen in the downward configuration if compared with the results for the upward configuration.

The temperature gradients were determined from the experimental values of cooling rate and growth rate, i.e. $G = \dot{T}/V$ (Fig. 4). The results obtained for downward solidification of the Al–3.2 wt% Bi alloy do not permit this kind of determination since such relationship is valid if thermal conduction is the sole heat transfer contribution, which is not the case in the downward configuration where convection currents are induced due to density differences between the two coexisting liquid phases.

The macrostructures of the directionally solidified castings are shown in Fig. 5. It can be seen that columnar growth has prevailed along the entire length of all alloys castings.

Typical microstructures are shown in Figs. 6 and 7. Fig. 6 shows cross- and longitudinal sections along the upward directionally solidified Al–2.0 wt% Bi alloy casting. It can be seen that cellular growth prevailed along the entire casting. The water-cooled mold imposes higher values of cooling rates close to the casting cooled surface and a decreasing profile along the casting length due to the increasing thermal resistance of the solidified shell with increasing distance in casting. This influence translates to the final as-cast microstructure, which results in coarser cells at positions far from the casting bottom.

The evolution of the Bi particles along the upward solidified monotectic Al–3.2 wt% Bi alloy casting can be found in a previous study by the same authors [13]. Fig. 7 shows the microstructures corresponding to the Al–3.2 wt% Bi alloy solidified downwards.

The morphology of Bi particles can be explained by the stability diagram proposed by Ratke and Müller [7,8], where the stability limit of fibers has been defined as a function of temperature gradients (varying from 2 K/mm to 11 K/mm) and solidification velocities

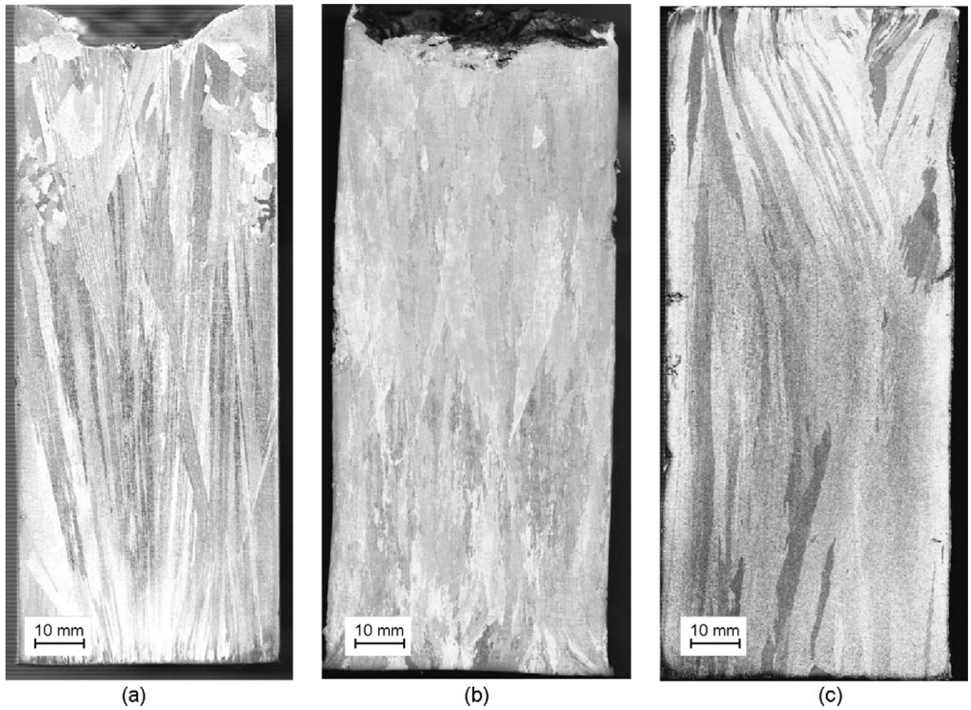

Fig. 5. Macrostructures: (a) Al–2.0 wt% Bi, (b) Al–3.2 wt% Bi alloys solidified upwards and (c) Al–3.2 wt% Bi alloy solidified downwards.

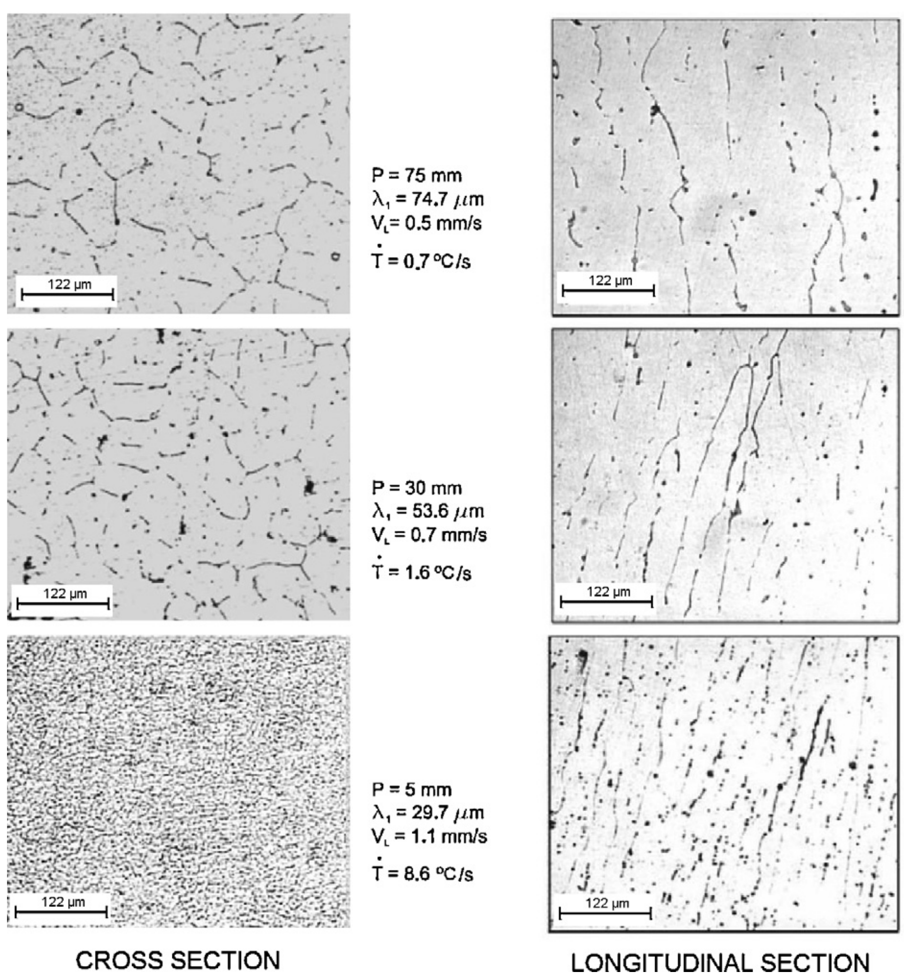

Fig. 6. Transversal and longitudinal microstructures of the upward directionally solidified Al–2.0 wt% Bi alloy casting. *P* is the position from the casting cooled surface; λ_1 is the average cell spacing; V_L is the tip growth rate and $\dot{T}$ is the cooling rate.

(from 0.3 μm/s to 6.0 μm/s). They suggested that either pearls of Bi droplets or irregular structures should prevail for larger solidification velocities or smaller gradients. If low velocities or large gradients are imposed, Bi fibers are expected to occur.

Tip growth rate and tip cooling rate dependences on cellular spacings of the Al–2.0 wt% Bi alloy are shown in Fig. 8, where average spacings along with the standard variation are presented. The lines represent empirical power laws which fit the experimental points. The cell spacing variation with cooling rate and tip growth rate are characterized by −0.55 and −1.1 power laws, respectively. The same exponents were reported by Rocha et al. [24], Goulart et al. [25] and Rosa et al. [26] concerning the cellular growth of Sn–Pb, Al–Fe and Pb–Sb alloys directionally solidified under unsteady-state conditions. This is in good agreement with the observations of Bouchard and Kirkaldy [27], which have concluded that for unsteady-state heat flow conditions an exponential relationship $\lambda_1 = \text{constant}\,(\dot{T})^{-0.50}$ best generates the existing experimental results.

Fig. 9a compares the experimental cellular spacings as a function of tip growth rate with the theoretical predictions from the Hunt–Lu model. In general, the experimental scatter lies below

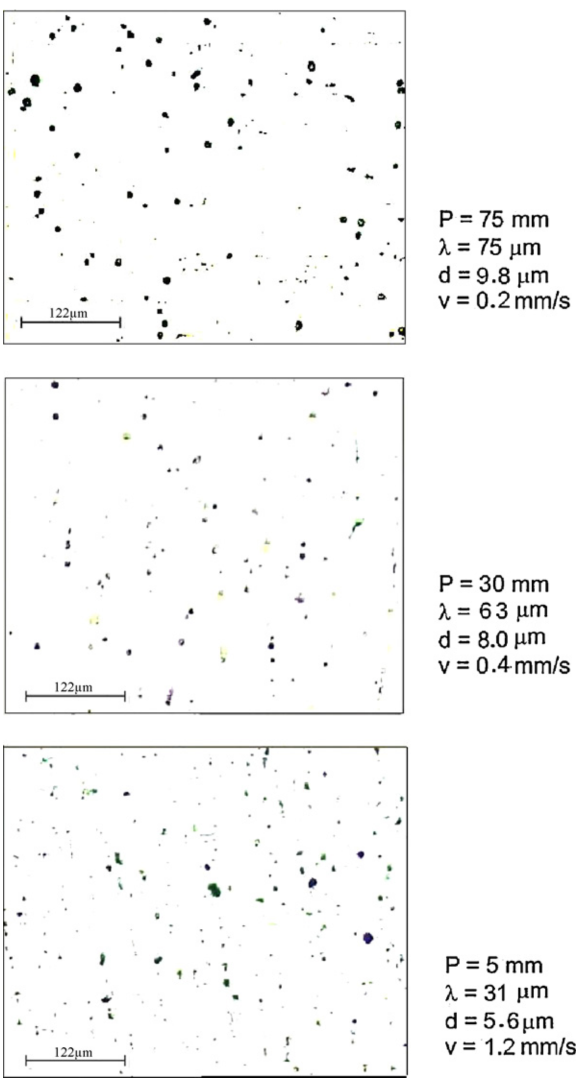

Fig. 7. As-cast longitudinal microstructures along the casting length of the downward directionally solidified monotectic Al–3.2 wt% Bi alloy casting. P is the position from casting cooled surface; λ is the average interphase spacing; v is the growth rate and d is the average diameter of Bi particles.

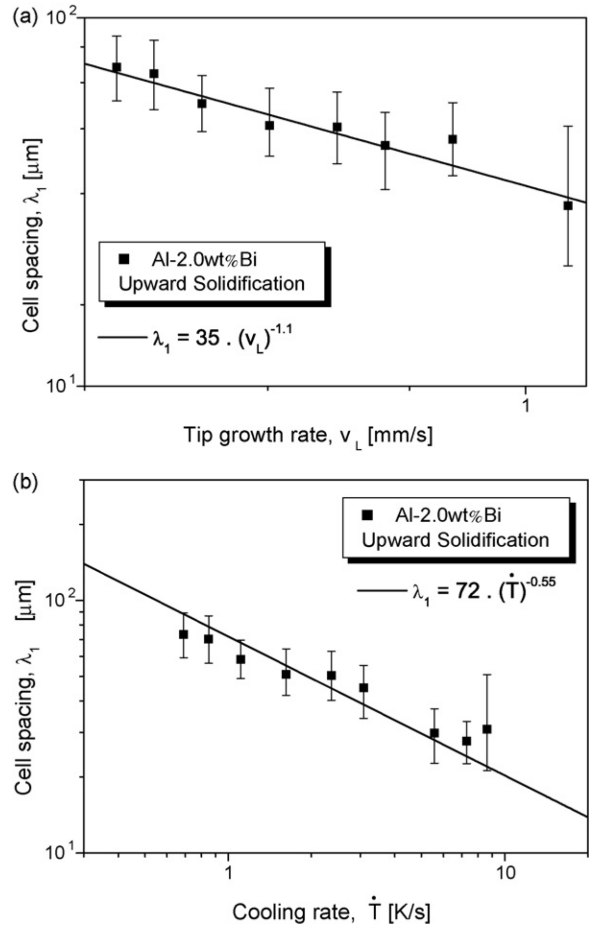

Fig. 8. Cellular spacing as a function of (a) tip growth rate and (b) tip cooling rate for the Al–2.0 wt% Bi alloy solidified upwards.

the minimum and maximum range of theoretical values predicted by such model. Goulart et al. [25] carried out upward directional solidification experiments with hypoeutectic Al–Fe alloys. After comparing their results with the Hunt–Lu model, they found that the maximum and minimum predictions had also overestimated the experimental scatter.

In order to analyze how the main steady-state theoretical predictive cellular growth models perform against experimental results of unsteady-state solidification, a comparison is made in Fig. 9b. It can be seen that the experimental scatter lies between the calculations performed with Kurz–Fisher's model and Hunt's model, and is closer to the theoretical predictions given by Trivedi's model for any composition experimentally examined. Goulart et al. [25] have also reported a good agreement with Trivedi's model for hypoeutectic Al–Fe alloys.

Fig. 10 shows the experimental values of the interphase spacing measured from the upward and downward solidified Al–3.2 wt% Bi alloy castings as a function of growth rate. Points are experimental results and lines represent an empirical fit to the experimental points, with spacings being expressed as a power function of growth rate. A single experimental law is able to represent both experimental scatters and, as a consequence, it was found a mean C value of 1.5×10^{-12} in order to fit the classical relationship used for eutectics: $\lambda^2 v = C$ (constant).

The experimental scatter of the downward solidified samples permitted to extend the total range of velocities where monotectic features could be observed. A slight difference between upward and downward monotectic growth may be noted in Fig. 10 if only the average interphase spacing values were taken into account. How-

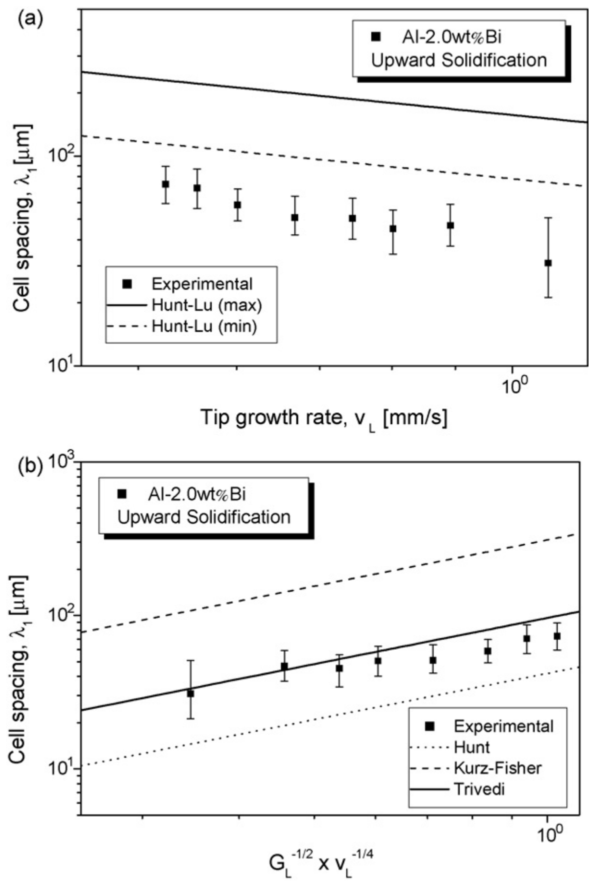

Fig. 9. Experimental and theoretical values of cellular spacing as a function of (a) tip growth rate and (b) $G_L^{-1/2} \times V_L^{-1/4}$ for the upward directionally solidified Al–2.0 wt% Bi alloy.

ever, if the minimum and maximum limits of λ are considered, a sole experimental law can be defined to represent both physical configurations, which seems to indicate that the effect of thermosolutal convective flow on the interphase spacing of a monotectic Al–3.2 wt% Bi alloy is not significant, as far as the interphase spacing is concerned.

As discussed in a previous work [13], such *C* value is higher than other *C* values found for monotectic growth [7,8,10–12]. It can be explained as a consequence of much higher velocities imposed by the present experimental solidification systems, which were designed to permit non-steady-state heat flow conditions to be attained. In these solidification systems, the Marangoni convection effect would induce fluid flow, which could induce a significant effect on the microstructure, i.e. the microstructural arrangement would depend on the concurrent action of the nucleation and diffusional growth of droplets, on the collisions and coagulations and on the spatial phases separation due to the Stokes and Marangoni effects [5,28,29]. Thus, the coarsening microstructural aspect found both in the Al–3.2 wt% Bi upward and downward solidified samples seems to be a result of the quick motion of the Bi-rich particles, causing collisions and coagulations between droplets. The coarsening of droplets leads to an increase in the interphase spacing typically found for transient solidification conditions. This seems to explain the present experimental results, which were characterized by a *C*-value of the growth law ($\lambda^2 v = C$) which is larger than those found for growth under steady-state conditions characterized by very low growth rates and where the mentioned convective effects seem to be less significant or even negligible.

Fig. 11 shows correlations between the Bi particles average diameter and the growth rate. As previously reported by Yang and Liu [11], a power function expression can define the droplet size distribution along the casting length. The maximum and minimum experimental limits reveal the diameter variation found for a same position in the casting. This seems to be related to the typical thermal instabilities of the solidification front, which are consequence of the transient regime of heat extraction. Likewise, Grugel and Helawell [12] proposed that oscillations in the growth front velocity caused by slightly unstable growth conditions could cause slight variations in the particles diameter.

It can be observed in Fig. 11 that coarser Bi-rich droplets were found in the upward case due to the sedimentation of phase L_2 (denser than L_1) towards the solidification front, while an opposite effect seems to happen during downward solidification of the Al–3.2 wt% Bi alloy casting. In this case, the Bi-rich droplets and L_2 tend to detach from the monotectic front, inducing a downward Bi flow. This will characterize a Bi-poorer liquid at the monotectic front and finer Bi particles will prevail in the final microstructure. The collective downward movement of droplets causes bismuth enrichment at the bottom of the casting. Fig. 12 shows a schematic representation of both cases, emphasizing the bismuth distribution in the remaining liquid during upward and downward solidification. It is well known that the magnitude of the Bi-rich particles is closely dependent on the compatibility between the kinetics of the solidification front and the movement of the Bi-rich particles. If such displacements are of the same order of magnitude, the solidi-

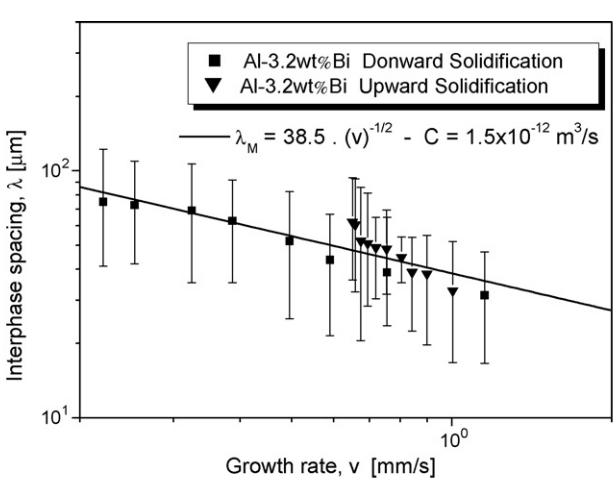

Fig. 10. Interphase spacing of the Al–3.2 wt% Bi alloy as a function of growth rate. λ_M refers to an average interphase spacing.

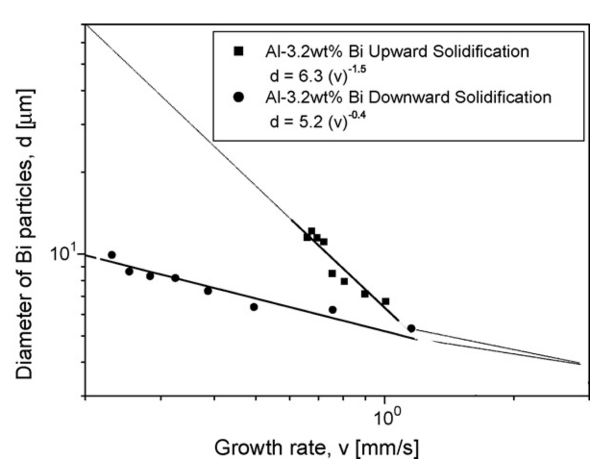

Fig. 11. Diameter of Bi droplets versus growth rate.

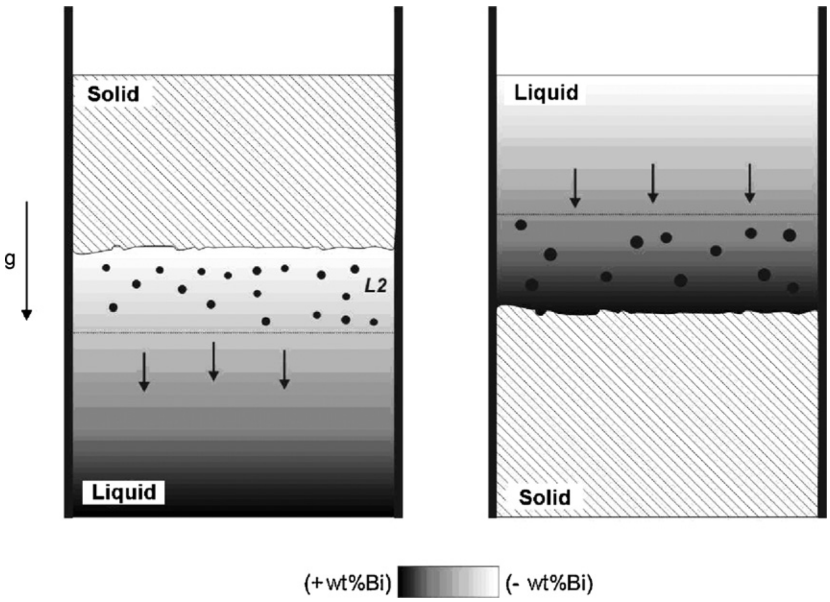

Fig. 12. Schematics of Bi-rich droplets behavior during (a) downward and (b) upward monotectic growth. *g* is the gravity vector.

fication front can incorporate the particles even before they achieve the bottom of the casting.

The solidification progress is quite similar in both evaluated situations (upward and downward configurations), which suggests that nucleation rate will be very similar along the solidification front. Such nuclei will originate the Bi-rich droplets. The interphase spacing is measured as a mean distance between the formed droplets. Hence, a significant variation in both interphase spacing evolutions for upward and downward solidified Al–3.2 wt% Bi alloy is not expected to be found. However, important differences can be noted concerning the Bi-rich particle size, with smaller particles characterizing the Al–3.2 wt% Bi solidified downwards.

Aoi et al. [15] reported that the resultant monotectic Cu–Pb microstructure does not depend on the growth direction, which seems to be in contradiction with the present results. On the other hand, Yang and Liu [11] reported that the diameter of Bi fibers decreased when a transverse magnetic field was applied during growth, and the microstructure became more homogeneous.

5. Conclusions

Bi droplets embedded into the aluminum matrix prevailed along Al–3.2 wt% Bi monotectic alloy castings solidified upwards and downwards. The non-steady solidification has favored the formation of structures which are coarser than those typical of steady-state experiments. The resulting $\lambda^2 v$ growth law is about two orders of magnitude higher than those for the steady-state regime. The interphase spacing behavior is the same for both solidification configurations, which leads to conclude that convective effects on the interphase spacing of the monotectic Al–3.2 wt% Bi alloy are not significant when such structural parameter is concerned. In contrast, the droplet size distribution along the casting length can be defined by a power function expression and a reduction on the size of the particles has been observed as a consequence of the gravity-induced sedimentation, which favored Bi enrichment at the bottom of the downward solidified casting.

Cellular microstructures prevailed along the Al–2.0 wt% Bi alloy casting length and no cellular/dendritic transition was detected. The cell spacing variation with cooling rate and tip growth rate were characterized by −0.55 and −1.1 power laws, respectively. When comparing the experimental cellular spacing as a function of tip growth rate with the unsteady (Hunt–Lu) and steady-state (Hunt, Kurz–Fisher and Trivedi) theoretical predictive cellular growth models, it was found that Trivedi's model resulted in better agreement with the experimental results. Hunt's model has underestimated the experimental values while Kurz–Fisher and Hunt–Lu's models overestimated the experimental scatter.

Acknowledgments

The authors acknowledge financial support provided by FAPESP (The Scientific Research Foundation of the State of São Paulo, Brazil), CNPq (The Brazilian Research Council) and FAEPEX-UNICAMP.

References

[1] G. Phanikumar, P. Dutta, R. Galun, K. Chattopadhyay, Mater. Sci. Eng. A 371 (2004) 91–102.
[2] H. Yasuda, I. Ohnaka, S. Fujimoto, N. Takezawa, A. Tsuchiyama, T. Nakano, K. Uesugi, Scripta Mater. 54 (2006) 527–532.
[3] H. Yasuda, I. Ohnaka, S. Fujimoto, A. Sugiyama, Y. Hayashi, M. Yamamoto, A. Tsuchiyama, T. Nakano, K. Uesugi, K. Kishio, Mater. Lett. 58 (2004) 911–915.
[4] R.N. Grugel, T.A. Lograsso, A. Hellawell, Metall. Trans. A 15 (1984) 1003–1012.
[5] J.Z. Zhao, J. He, Z.Q. Hu, L. Ratke, Z. Metallkd. 95 (2004) 362–368.
[6] A. Ludwig, M. Wu, A. Abondano, L. Ratke, Mater. Sci. Forum 508 (2006) 193–198.
[7] L. Ratke, A. Müller, Scripta Mater. 54 (2006) 1217–1220.
[8] L. Ratke, Mater. Sci. Eng. A 413–414 (2005) 504–508.
[9] T. Carlberg, A. Bergman, Scripta Metall. 19 (1985) 333–336.
[10] B. Derby, J.J. Favier, Acta Metall. 31 (1983) 1123–1130.
[11] S. Yang, W. Liu, J. Mater. Sci. 36 (2001) 5351–5355.
[12] R.N. Grugel, A. Hellawell, Metall. Trans. 12A (1981) 669–681.
[13] A.P. Silva, J.E. Spinelli, A. Garcia, J Alloy Compd., in press. doi:10.1016/j.jallcom.2008.07.021.
[14] L. Ratke, Metall. Mater. Trans. 34A (2003) 449–457.
[15] I. Aoi, M. Ishino, M. Yoshida, H. Fukunaga, H. Nakae, J. Cryst. Growth 222 (2001) 806–815.
[16] M. Reuβ, L. Ratke, J. Zhao, Mater. Sci. Forum 508 (2006) 37–44.
[17] J.D. Hunt, International Conference on Solidification and Casting of Met als, The Metals Society, London, 1979, pp. 3–9.
[18] W. Kurz, J.D. Fisher, Acta Metall. 29 (1981) 11–20.
[19] W. Kurz, J.D. Fisher, Fundamentals of Solidification, Trans Tech Public, Switzerland, 1992, pp. 85–90.
[20] R. Trivedi, Metall. Mater. Trans. 15A (1984) 977–982.
[21] J.D. Hunt, S.Z. Lu, Metall. Mater. Trans. 27A (1996) 611–623.

[22] J.E. Spinelli, I.L. Ferreira, A. Garcia, J. Alloy Compd. 384 (2004) 217–226.
[23] M. Gündüz, E. Çardili, Mater. Sci. Eng. A 327 (2002) 167–185.
[24] O.L. Rocha, C.A. Siqueira, A. Garcia, Mater. Sci. Eng. A 361 (2003) 111–118.
[25] P.R. Goulart, K.A.S. Cruz, J.E. Spinelli, N. Cheung, I.L. Ferreira, A. Garcia, J. Alloys Compd. 470 (2009) 589–599.
[26] D.M. Rosa, J.E. Spinelli, I.L. Ferreira, A. Garcia, J. Alloys Compd. 422 (2006) 227–238.
[27] D. Bouchard, J.S. Kirkaldy, Metall. Mater. Trans. 28B (1997) 651–663.
[28] J.Z. Zhao, L. Ratke, Scripta Mater. 50 (2004) 543–546.
[29] L. Ratke, J. Alkemper, Adv. Colloid Interf. Sci. 58 (1995) 151–170.